Diagnostic and Interventional Imaging (2013) **94**, 925—943

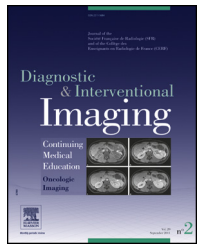

CONTINUING EDUCATION PROGRAM: FOCUS...

Post-traumatic brachial plexus MRI in practice

O. Silbermann-Hoffman[a,*], **F. Teboul**[b]

[a] *American Hospital of Paris, 63, boulevard Victor-Hugo, 92200 Neuilly-sur-Seine, France*
[b] *Peripheral nerve and Brachial Plexus Institute of Surgery, 92, boulevard de Courcelles, 75017 Paris, France*

KEYWORDS
MRI;
Post-traumatic brachial plexus paralysis;
Avulsion;
Nerve rupture;
Axillary nerve neuroma

Abstract Injuries are separated into spinal nerve root avulsions (pre-ganglionic lesions) and more distal rupture (post-ganglionic lesions). The lesions may be associated with different nerve root levels. Spinal MRI is used to diagnose pre-ganglionic lesions, which may be present in the absence of pseudomeningoceles. The other sequences described are used to diagnose post-ganglionic lesions, regardless of the type of lesion. Knowledge that a graftable C5 nerve root is present is important in the treatment strategy. Contrast enhancement in the scalene triangle does not predict the quality of the nerve root (continuous injury with response to peroperative stimulation or division of the root needing grafting). Understanding post-traumatic neuronal injuries to the brachial plexus. Knowing how to look for spinal MRI abnormalities and post-ganglionic abnormalities.

Traumatic brachial plexus paralysis in adults mostly affects young people between 20 and 30 years old. Ninety percent of cases are due to motorbike accidents. The mechanism of the injury involves stretching of the brachial plexus nerves which may lead to two types of damage: avulsion, or tearing off of the insertion of the nerve roots from the spinal cord (pre-ganglionic lesion) and nerve rupture within the brachial plexus (post-ganglionic lesion). The neuronal injury may affect the nerve roots making up the brachial plexus in the scalene triangle, and also in the plexus' trunks, bundles and terminal branches. Post-ganglionic injury often leads to a neuroma in continuity. Occasionally a clean rupture occurs, causing nerve retraction. The investigation and treatment of these injuries are relatively urgent and recent publications have shown the essential role of the pre-operative interval (less than 6 months) in recovery. Clinical examination combined with electrophysiological and MRI studies enable surgeons to optimize their treatment strategy.

* Corresponding author.
E-mail address: Olivia.silbermann@yahoo.fr (O. Silbermann-Hoffman).

2211-5684/$ — see front matter
http://dx.doi.org/10.1016/j.diii.2013.08.013

Individual investigations completed in isolation are inadequate. MRI is the first line imaging investigation: spinal CT is used if it is not possible to perform this. MRI can accurately diagnose pre-ganglionic and confirm post-ganglionic injuries, although usually cannot assess whether these lesions have the potential to recover, i.e. establish whether or not post-ganglionic injuries have the capacity to recover function. Functional capacity is assessed by changes in signs of renervation on repeated electromyograms. If no signs of renervation are seen at 3 months, surgery is required, as it is with lesions, which partially recover on several repeated EMGs. If a direct surgical approach is used, palpating and electrostimulating the nerves can confirm or exclude their functional capacity.

Anatomical review

The brachial plexus is made up of the anterior branches of the C5 to T1 nerve roots, with a possible component coming from the C4 and T2 roots. The nerve roots consist of anterior and posterior branches, which meet at the foramen and extra-foramen junction to form a single nerve root, which divides into an anterior branch, which forms part of the brachial plexus, and a posterior branch, which innervates the paravertebral muscles. Each anterior and posterior nerve root branch is formed by the union of several rootlets, which arise directly from the spinal cord, well before the nerve leaves the foramen (Fig. 1a). These rootlets consist of three or four bands from C5 to C7 and two bands in C8 and T1 [1] with a large number of rootlets for the posterior part. The spinal ganglion, located in the region of the foramen (Fig. 1b), arises from the posterior part and is the origin of the sensory fibers, and the anterior part carries the motor fibers. The brachial plexus is divided into five different anatomical parts; the roots, trunks, division of the trunks, bundles and terminal branches. The roots pass down through the scalene triangle between the anterior and middle scalene muscles. They then join and form trunks in the lateral part of the scalene triangle. The superficial trunk is formed from the union of the anterior roots of C5 and C6 and gives rise to an important branch, the suprascapular nerve. The middle trunk is a continuation of the anterior root of C7 and the inferior trunk arises from the union of the anterior roots of C8 and T1. The trunks arise from the lateral aspect of the middle scalene muscle. A landmark that should be sought out on coronal sections is the dorsal scapular artery, a branch of the subclavian artery, which passes between the superior and middle trunks or between the middle and inferior trunks [2,3]. Each trunk gives rise to two divisions, one anterior and one posterior, which lead to in six divisions originating where these neuronal bundles cross the clavicle (costoclavicular junction), which then group into bundles. The lateral bundle arises from the anterior divisions of the superior and middle trunks, the medial bundle from the anterior division of the inferior trunk and the posterior bundle from the posterior divisions of all three trunks. Each bundle then leads on to several terminal branches. The main branches of the lateral bundle are the musculocutaneous nerve and the lateral root of the median nerve. The medial bundle gives rise to the ulnar nerve and the medial root of the median nerve, and the posterior bundle to the radial nerve and the axillary nerve.

MRI myelography clearly shows the posterior nerve root component, which contains more rootlets than the anterior component, and the smaller number of nerve rootlet bands in C8-T1. The rootlets leave the spine, carrying with them the dura mater and arachnoid membrane. The dura mater and arachnoid stop at the foramina, when the dura mater extends and merges with epineurium whereas the outer layers of the arachnoid membrane fuse with the perineurium [4] which adheres to the anterior nerve root and

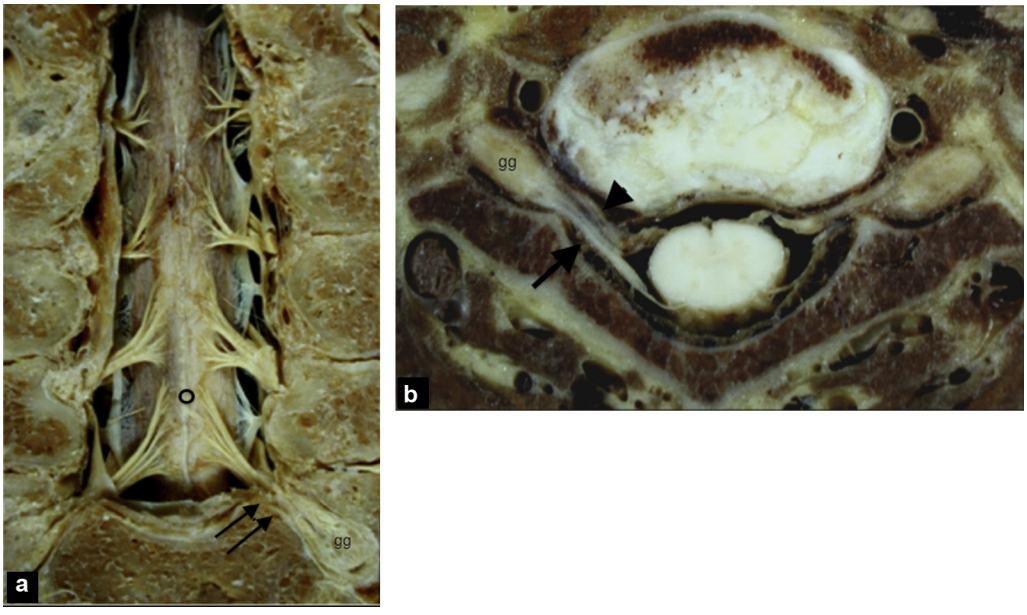

Figure 1. Anatomical sections by Prof. Demondion: a: the roots emerge from the spine (round) proximal to their emergence from the foramen (double arrow); b: the spinal ganglion (gg) is continuous with the posterior rootlets (arrow) behind the anterior rootlets (arrow head).

spinal ganglion, explaining why CSF is not seen in the foramen unless an arachnoid diverticulum (a variant of the norm) or post-traumatic lesion is present. Pseudomeningoceles are due to extravasation of CSF through a breach, forming an unencapsulated pouch of fluid.

Assessment of neurological functions

Clinical examination

The patient's neurological injuries should be assessed promptly via a full examination in order to establish whether or not he/she is a candidate for surgery. The earlier a patient is examined, the more likely it is that the prognosis of the lesions can be established (stable damage, recovery or deterioration). Upper limb paralysis secondary to the stretching of the nerves may be complete (75%) or partial (25%). The injuries are supraclavicular in 72% of cases and infraclavicular in 28% of cases [5]. Overall, 25% of plexus injuries involve complete avulsions. Fifteen percent of patients with supraclavicular injuries have concomitant distal retro- and/or infraclavicular damage [6]. Various clinical pictures can be distinguished, depending on the nerve roots concerned, although, despite the fact that each nerve root corresponds to a muscle group, the distribution of nerve fibers occasionally varies. Muscles may be innervated by different nerve roots in different patients (for example, the radial nerve may receive most of its fibers from C7, which is usually the case, although occasionally from C8 or even T1). Damage to C7 may therefore occur without defective elbow and wrist or finger extension, and it is therefore more appropriate to describe the paralysis according to the affected function (paralysis of the shoulder, elbow flexion, wrist extension etc.). Restoring elbow and shoulder mobility is the key objective.

Imaging and neurophysiological studies (nerve conduction and electromyography) are essential to assess traumatic brachial plexus paralyses in order to assess the level of the lesion, type of neuronal damage and potential for recovery.

Neurophysiological studies

A certain level of knowledge is required to understand the results of this investigation. Seddon produced a functional classification of nerve injuries in 1942 [7] separating injuries into neuropraxia, axonotmesis and neurotmesis. Neuropraxia involves loss of nerve function, causing conduction block but without anatomical injury. Recovery may take up to 12 weeks. Axonotmesis is secondary to axonal rupture without damage to the Schwann linings, which results in distal Wallerien regeneration with slow functional recovery as the endoneurial tubes are preserved. Thirdly, neurotmesis involves division of all of the parts of the nerve (damage to the axons and linings), in which case no recovery occurs.

Neurophysiological study should not be performed less than 4 weeks after the injury (the Wallerien degeneration time) with repeat studies at 6-week intervals. Sensory potentials can differentiate between pre- from post-ganglionic injury. The sensory neuron cell body is located in the posterior ganglion at the foramen, and in a pre-ganglionic injury (avulsion) the ganglion remains intact. Complete clinical lack of sensation is found in the territory investigated, with preserved sensory nerve potential amplitudes. On the other hand, a mixed pre- and post-ganglionic injury cannot be excluded if these potentials are reduced. The extent of muscle denervation and number of functional motor neurons is established by ELG. A motor unit is made up of the motor neuron cell body, its axon and all of the muscle fibers, which it innervates, and is responsible for bi- or tri-phasic waves. The resting trace of a normally innervated muscle is flat. Muscle contraction leads to the appearance of spikes, the number and appearance of which depend on the contraction force — i.e. the number of motor units used. A denervated muscle exhibits short, low potentials on the resting trace, which develop approximately 3 weeks after the accident, i.e. once the axons have completely degenerated (these are known as ''fibrillation potentials''). In addition, intentional attempts to contract the muscle, or stimulation of the nerve, do not trigger spikes. Neuronal regeneration results in a fall in the fibrillation potentials and the emergence of regeneration potentials after intentional attempts to contract the muscle. The presence of polyphasic resting fibrillation waves, which indicate denervation, and poor voluntary contraction traces indicate a lack of functional units. Signs of re-innervation develop between 2 and 4 months after the injury.

MRI

The modified Nagano classification of brachial plexus injuries describes four zones. Zone I involves the avulsion of rootlets from the spine; zone IIA contains ganglion injuries within the foramen; zone IIB comprises the nerve roots up to the division of the trunks; zone III when the injured area involves the trunks; and zone IV when the centre of the injury is on the bundles [8]. Zone IIA is defined as a post-ganglionic injury, although it is, in fact, the equivalent of avulsion as it is too proximal to be grafted.

Pre-ganglionic injuries

There are both direct and indirect signs suggesting pre-ganglionic damage. These injuries are studied by investigating the rootlets, analyzing meningeal linings, any contrast enhancement on the path of a nerve or on the surface of the spine [9] and by examining the paravertebral muscles [10].

Spinal CT has long been the reference investigation for these injuries. Published results have shown equivalent sensitivity and specificity results when they are investigated by MRI if high quality myelography sequences are taken, providing excellent contrast between CSF and the rootlets, combined with excellent spatial resolution. Sensitivity ranges between 89% and 96.1% against the ''gold standard'' of spinal CT with a specificity of between 95 and 96.6% [11—13]. Myelography MRI is named differently depending on the manufacturers (Gradient 3D Echo: fiesta [GE] CISS [Siemens] True-Fisp [Philips]; Ultra Fast Spin Echo T2: SSFSE [GE] SSTSE [Haste Siemens] SSIT-TSE [UFSE

Philips]). These enable volume acquisition with secondary reconstructions in the different spatial planes. This type of sequence is essential for detailed analysis of pre-ganglionic lesions and should be repeated if artefacts are produced as a result of movements.

We use the 3D FIESTA sequence (T2/T1 ratio), which provides high signal to noise images with few flow artefacts, although this sequence is sensitive to swallowing and movement artefacts. In addition, the bone marrow and spinal cord appear very black restricting the examination of the vertebrae and for spinal edema [14] and only offering good analysis of the rootlets in 60% of patients because of multiple large pseudomeningoceles. The same occurred with spinal CT. These large pseudomeningoceles are rarely seen now, probably because accidents are at lower speeds (radar speed traps, license penalty points). We record our images in the sagittal plane, although other groups use frontal or axial planes [15] with the patient lying on his/her back, arms along the length of the body, and with their head and neck as straight as possible. A 21-phase array head and neck coil is used. The volume is placed on the axial ''scout view'', including the spinal cord and a proximal part of the foramina (Fig. 2a) using the following settings: TR = 5.5, TE = min full. Field 22 cm, matrix 288 × 320 antero-posterior frequency, 52 loc, 3 excitations, flip angle 45°, band width 62.5 section thickness 0.8 mm or 1 mm. The patient is asked to breathe gently, using their stomach, and to try not to swallow during the acquisition. Axial reconstructions are made from the volume recorded in the middle plane of the discs from C4 to T1-T2 in 1 mm thicknesses with an interval of 0.5 mm (Fig. 2b). This results in approximately 200 sections, which can be seen in cine mode on the console. The direct signs observed are whether or not the rootlets arising from the spinal cord, which leave through the foramen are visible, and spinal signal abnormalities at the point of insertion of the rootlets into the spinal cord or into the rootlets themselves.

Examination of the rootlets

Both the anterior and posterior rootlets can be torn off from the spinal cord at all levels (total avulsion) (Fig. 3a—d). Less commonly, all of the individual anterior or posterior rootlets are torn off (partial avulsion) (Fig. 4a—d). Some of the anterior and/or anterior and posterior rootlets (pauci-rootlet appearance) may occur (Fig. 5a—d) wherein the rootlets may be present but thickened (Fig. 6). Partial avulsion injuries are rare and were found in 4.6% (5 out of 105 rootlets) in Tsai's series [16] and in 5.6% in Gasparotti's series [17]. Oblique reconstructions are performed to identify the posterior rootlets (Fig. 7a), together with frontal and/or oblique reconstructions for the anterior rootlets (Fig. 7b). Summary films containing approximately six to eight images per nerve root level are given to the clinician with the nerve root levels annotated on them (Fig. 8a—h).

Examination of the meninges

Pseudomeningoceles are present in 80% of avulsions, i.e. approximately 20% of avulsions occur without forming pseudomeningoceles. In their series, Gasparotti et al. [11] reported five cases of pseudomeningoceles without nerve root abnormalities, something we have never seen. These pseudomeningoceles may be large or small (saccular or diverticular), immediately against the foramen, they may extend over several levels, or they may lie anterior or posterior peri-spinally (Fig. 9a—c).

Indirect signs

Rootlet contrast enhancement (12/250) (Fig. 10) or nodular contrast enhancement on the surface of the spinal cord (42/250) is rare and very suggestive of pre-ganglionic injuries (7/12 and 38/42) [9]. Spinal abnormalities may coexist with pre-ganglionic injuries in approximately 20% of cases, such as displacement of the spinal cord on the healthy side, spinal edema around the emergence of the rootlets

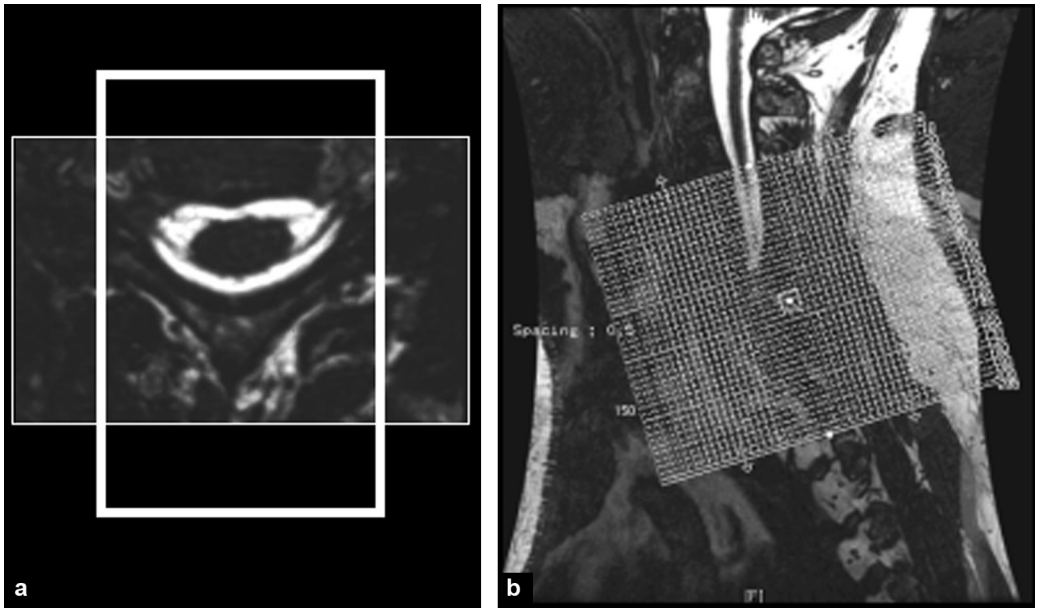

Figure 2. a: the 3D myelography image is positioned on the scout axial, represented here by an axial myelography section for better visibility; b: axial reconstructions from the sagittal volume are made in the middle plane of the discs of C4-C5 to C7-T1.

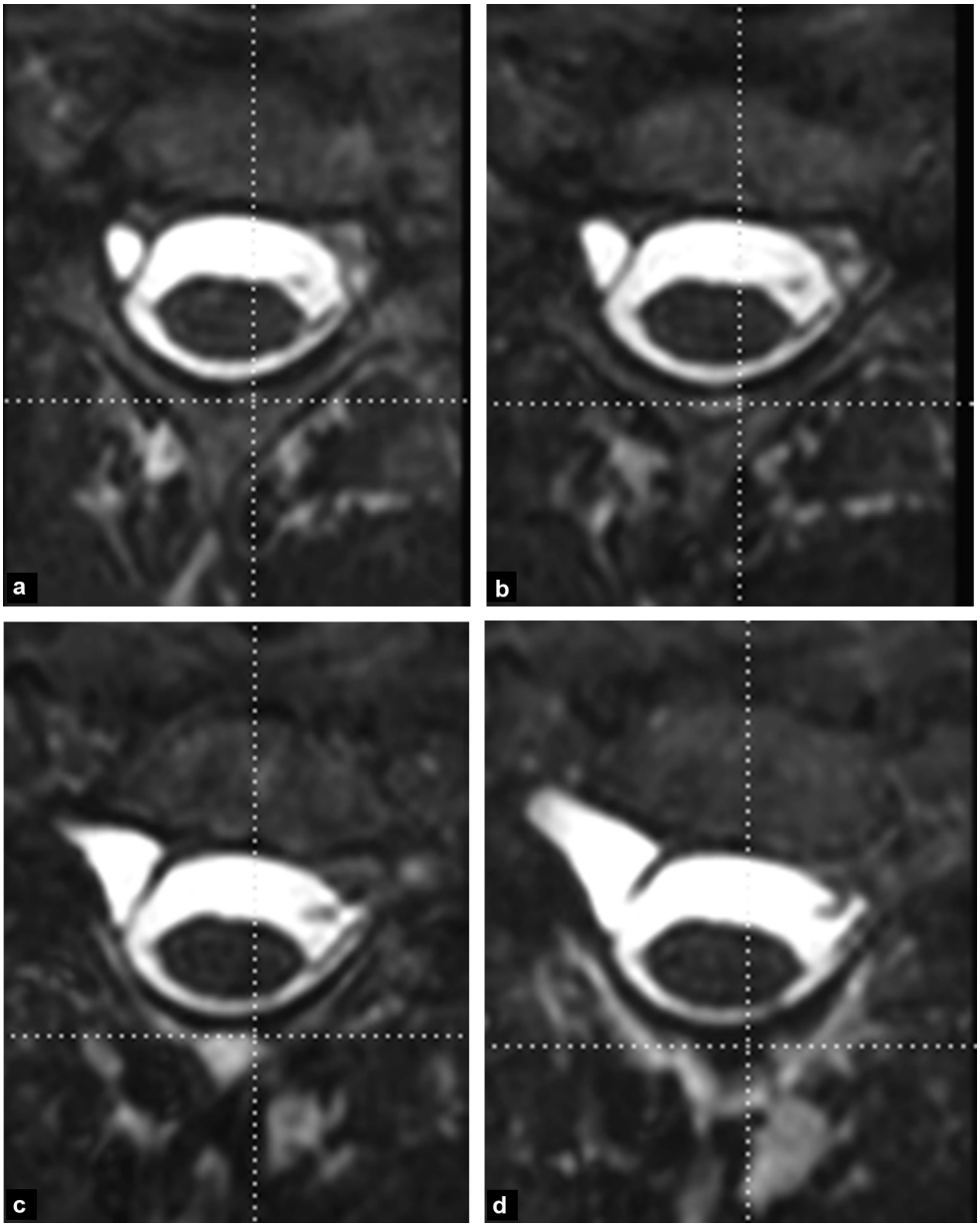

Figure 3. Total avulsion. Neither the right anterior or posterior rootlets can be seen, unlike the levels on the contralateral side (a—d). Note the pseudomeningocele.

or more widespread edema in the acute phase, myelomalacia occurring later, hemosiderin deposition; more rarely, a spinal defect (Fig. 11) [14].

Other signs supporting a pre-ganglionic lesion include muscle signal abnormalities, which should be examined for on T2, T1 and T1 gadolinium-enhanced weighted sequences. The muscle signal abnormalities involve contrast enhancement in 88% of cases (Fig. 12a, b), with a T2 hyperintensity compared to the normal muscles in 83% of cases, T1 weighted hyperintensity in 37%, amyotrophy in 78% and no abnormality in 12% of cases. These abnormalities affect posterior paravertebral muscles, particularly the multifidus [10]. The cervical nerve roots divide into an anterior and posterior root after the spinal ganglion. The anterior root joins the brachial plexus and the posterior root innervates the posterior paravertebral muscles, including the multifidus. A lesion proximal to the origin of this posterior branch can therefore cause denervation of these muscles, although neuronal anastomoses exist between the different levels (less commonly for the multifidus), which means that denervation signals are usually absent in incomplete multilevel injuries. Nodular contrast uptake with clear outlines represents uptake of contrast enhancement by the retracted spinal ganglion of the avulsed nerve root.

Post-ganglionic injuries

We shall firstly review the anatomy of the nerve and then review the protocol, which we use routinely to investigate scalene triangle injuries, behind and beneath the clavicle. We will then describe the protocol we use if we suspect axillary nerve damage.

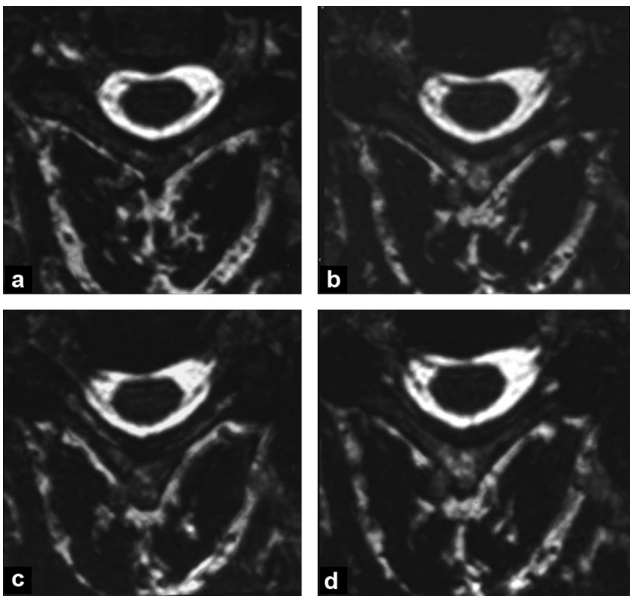

Figure 4. Partial avulsion of the left anterior rootlets, which are not visible at the different levels (a—d) from their emergence from the spine until they leave the foramina, unlike the posterior rootlets.

Figure 6. Sagittal myelography MRI sequence. Thickened appearance of the C5 posterior rootlets (red arrow) compared to the level just above it.

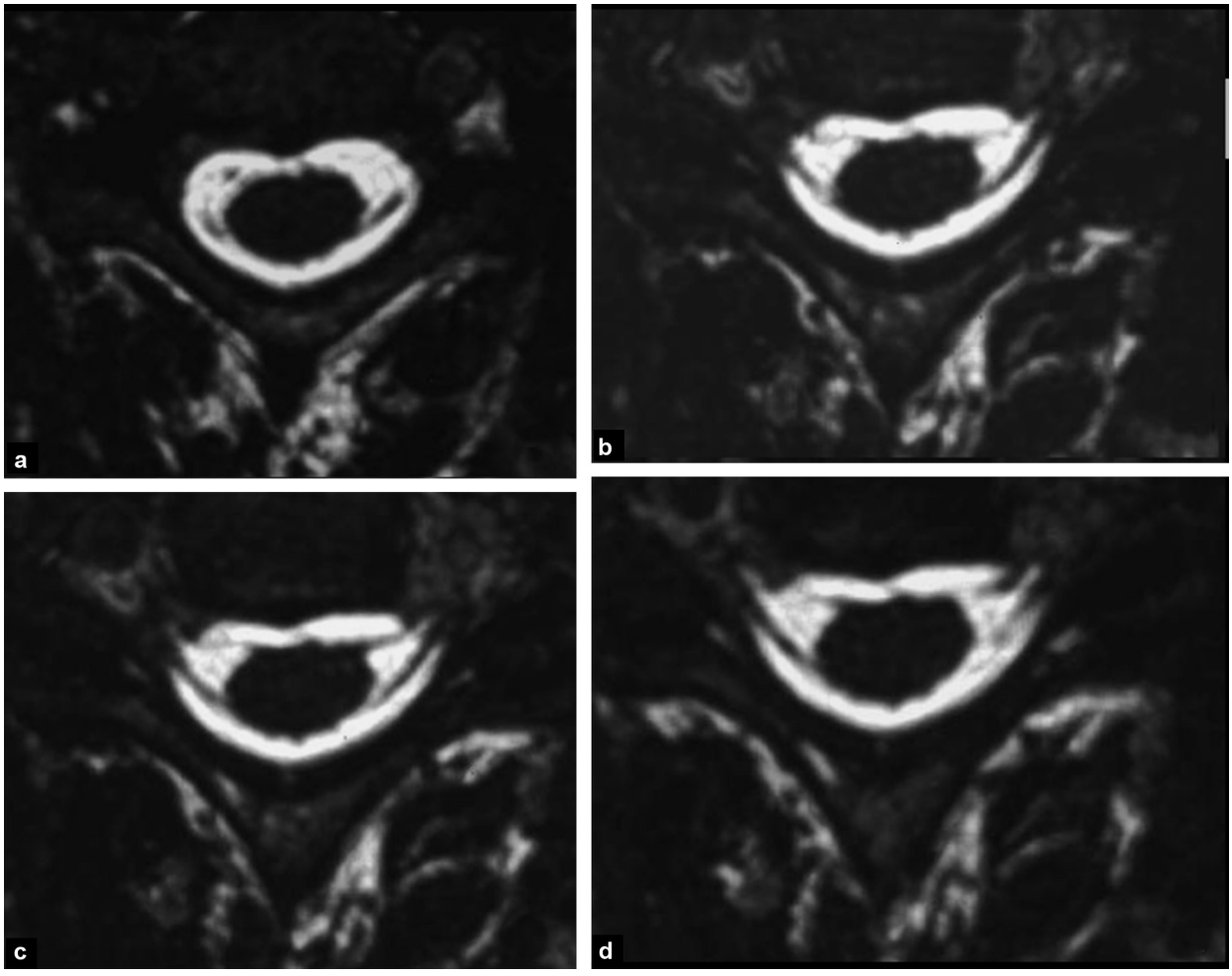

Figure 5. Pauci-rootlet appearance. The left anterior rootlets can be seen in b, c and d, but not in a.

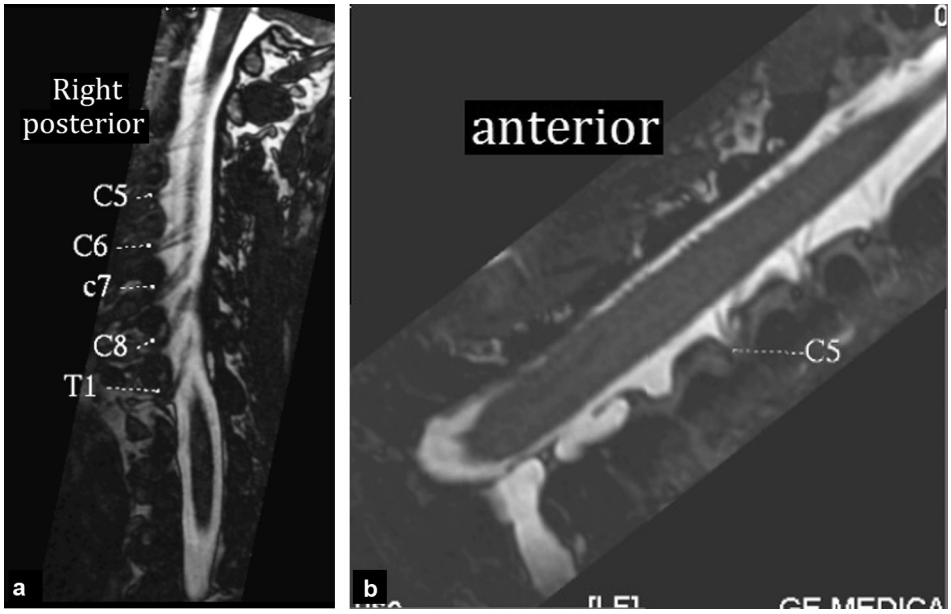

Figure 7. Oblique reconstructions of the myelography volume: a: the posterior rootlets are very clearly seen. Note the increasing oblique path of the rootlets from above downwards, with disappearance of the fanning of the rootlets, also from above downwards; b: there are fewer anterior than posterior rootlets.

Anatomical and physiological review

Mixed nerves are made up of axons, some myelinated some un-myelinated, which meet in nerve bundles. A bundle is made up of several axons, separated from each other by the endoneurium and demarcated by the perineurium. Nerves are made up of several bundles, separated by the epineurium, which thickens peripherally and forms the external boundary of the nerve. Blood vessels are present on the surface of the epineurium and within the epineurium between the bundles. Blood vessels are also present on the surface of the perineurium and within, in the endoneurium (Fig. 13). Anastomotic connections between the longitudinal epineural, perineural and endoneurial circulations occur at different levels through transverse anastomoses. Edema increases the hydrostatic pressure of the endoneurium (which naturally is positive at 2—3 mmHg) and may have an effect on these anastomoses. Direct and indirect exchanges occur at the neurovascular interface. The direct exchanges occur via the endothelium of the blood vessels located in the endoneurium, and the indirect changes occur via the epineurial vascular endothelium, via the capillary network in the extracellular space, and then via the perineurium in the endoneurium. These blood vessels consist of arterioles and venules. Exchange between the physiological space within the bundle and the extracellular space is restricted and regulated by the neurovascular barrier or neurovascular interface. This barrier is poorly permeable and insulates the endoneurium from rapid changes in concentrations of various plasma solutes, reducing the potential adverse effect on the Schwann cell and on axonal function. The lack of lymph drainage from the endoneurium increases the protective effect of this neurovascular interface [4,18]. Endoneurial flow occurs from the spine towards the periphery. The hydrostatic pressure in the spine is 10 mmHg, compared to approximately 3—5 mmHg in the dorsal root ganglion and 2—3 mmHg in the peripheral nerves. Following post-traumatic nerve injuries, Wallerien degeneration occurs, accompanied by an increase in perineural permeability, followed by a rise in endoneurial hydrostatic pressure. Increased endoneurial water content may persist when the endoneurial pressure returns to normal secondary to an increase in perineurial compliance [4]. Sunderland's histological classification of nerve injuries [18] describes five stages of increasing severity: stage 1 involves Seddon's functional neuropraxia (axonal continuity), stage 2 is axonotmesis (axonal rupture with intact Schwann cells), stage 3 involves coexistent damage to the endoneurium but no damage to the perineurium, stage 4 involves an interfascicular injury and stage 5 reflects nerve division (Seddon's neurotmesis). Functional recovery does not occur in stages 4 and 5.

Imaging

The lesions to look for are firstly an increase in nerve signal, whether or not this is accompanied by an increase in nerve volume, which may reflect a neural injury with continuity or simply endoneurial edema, retraction of the nerve in the scalene triangle, which may be due either to retraction of an avulsed nerve or neuronal rupture in the triangle (Fig. 14a—c) or intermittent or more diffuse contrast enhancement of the plexus (Fig. 15a, b). A muscle hyperintensity indicating a denervation signal should be looked for (Fig. 16).

Neuronal edema is identified on STIR or T2 fat suppression sequences.

Normal nerves appear as isointensity with muscle on T1 weighted sequences and isointense or slightly hyperintense in T2 weighted fat suppression sequences, not enhancing after gadolinium. Various diseases can result in more pronounced pathological rises in the nerve signal (trauma, inflammatory disease, compression or infiltration), secondary to an increase in nerve water content

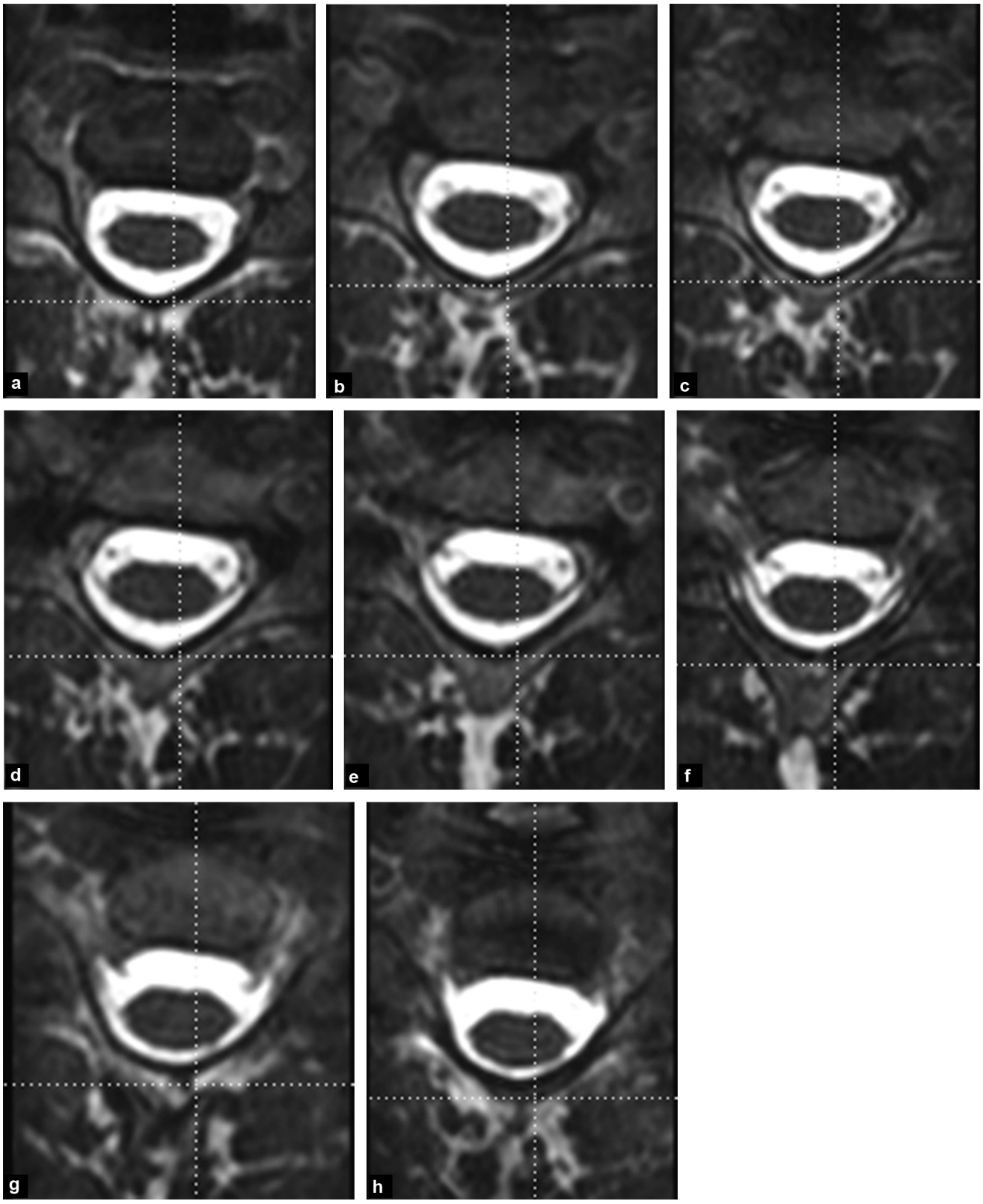

Figure 8. Normal myelography appearances: a—h: the rootlets are clearly visible from their emergence from the spine until they leave the foramina.

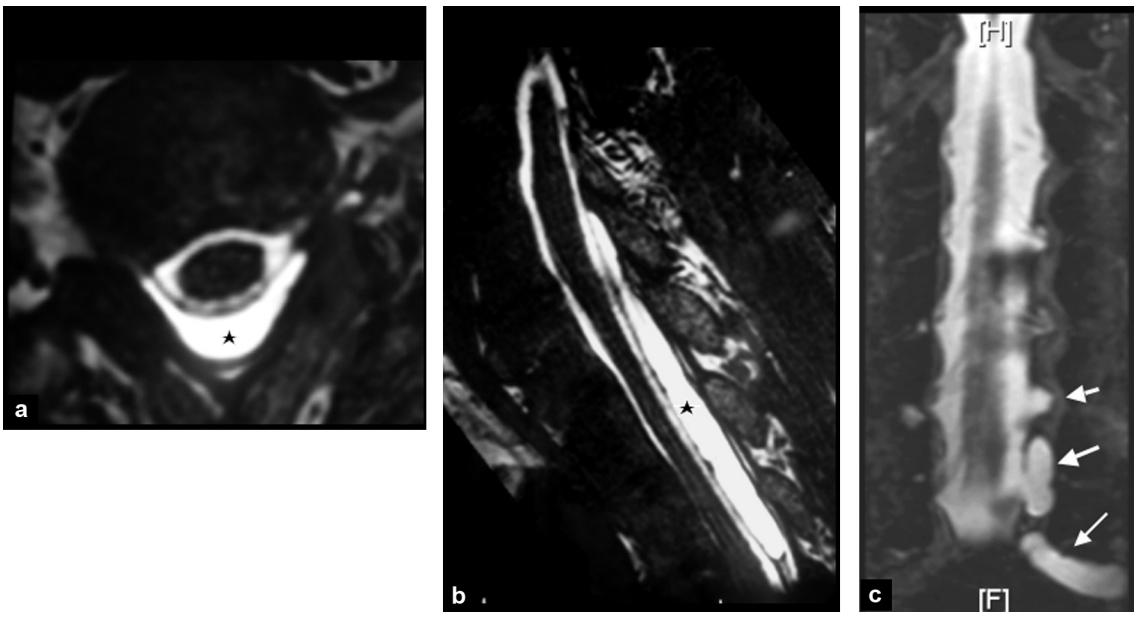

Figure 9. Large posterior peri-spinal pseudomeningocele (star), a: in the axial plane; b: in the sagittal plane; c: three different pseudomeningoceles (white arrows).

because of disturbance of endoneurial flow (Fig. 17). A T2 weighted hyperintensity may be due to a magic angle artefact (Fig. 18), which is well known in tendon imaging, and may incorrectly suggest disease (false positive) [19]. Nerves contain many collagen fibers and the orientation of the brachial plexus varies depending on the area of investigation (nerves, trunks or bundles) between 40 and 60° from the B_0 field. To avoid the magic angle artefact (55°/B_0) echo times of 40 ms should be used (between 70 and 100 ms) [20]. In addition, STIR hyperintensity in parts of the brachial plexus does not in any way predict the nature of the injury in the absence of a visible neuroma and clinical recovery may occur after several months [21]. The finding of a coexistent increase in diameter with hyperintensity may reflect a neuroma in continuity, which may or may not represent some intact fibers or adequate axonal regrowth.

Investigation protocol

STIR or T2 IDEAL weighted coronal and sagittal MRI

The coronal sequence is recorded in a plane parallel to the long axis of the spine (Fig. 19), field of vision 33 cm, 15 × 3.5 mm thick sections every 0.5, a matrix of 320 × 256, TR of 3111 and TE of 88.4. The sagittal sequence (Fig. 20) is recorded with a field of vision of 24 cm, 5 mm thick sections every 1, a matrix of 288 × 224, TR of 4689 and TE of 88.2. The first section is at the foramina. The benefit of IDEAL MRI (iterative decomposition of water and fat with echo-asymmetry and least-squares estimation) is that fat suppression is homogeneous (as the cervical region is anatomically difficult because of the cervical lordosis, which causes and air/tissue susceptibility artifact, and potentially artefacts due to dental metal), combined with a T2

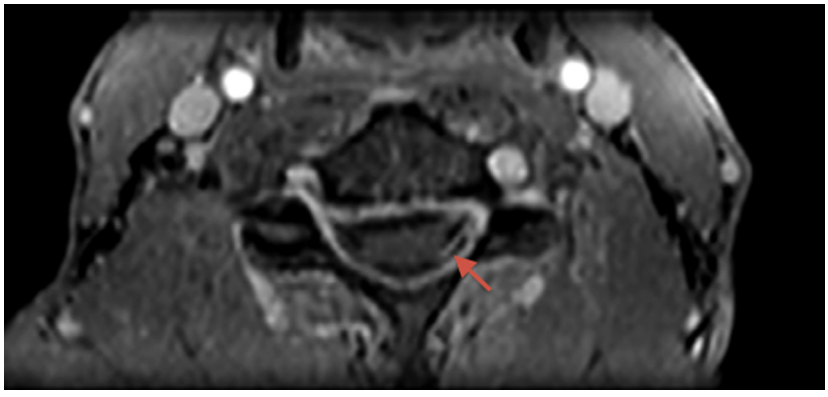

Figure 10. Contrast enhancement by rootlets (arrow) is a sign of pre-ganglionic damage.

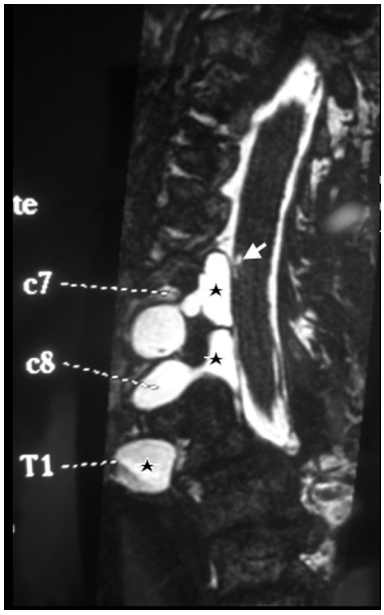

Figure 11. Spinal defect opposite to the area of former C7 rootlet emergence (white arrow) in a patient with total plexus paralysis. A C6 rootlet remains. The C5 rootlets just above have been avulsed. Large C7C8T1 pseudomeningoceles (star).

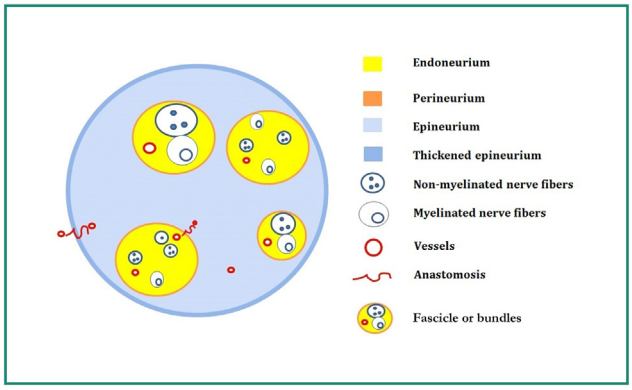

Figure 13. Anatomical diagram showing a peripheral nerve.

reconstructed sequence without fat suppression. This sequence is taken at three different echo times, which separates the water image from the fat image. Four weighted sequences are obtained from a water alone sequence (T2 fat sat image), a combined fat and water image sequence in phase (T2 weighted image), a combined fat and water out of phase image, and a fat only image (suppressing the water image). We take a single oblique coronal sequence, which does not image all of the scalene triangle roots in the same image because of the different oblique paths of these nerves. Sagittal sections allow the different roots to be followed, section-by-section, from the point where they leave the foramen, and to compare their image intensity and size and even their joining into a trunk at the level of the first rib, together with the division of the trunks and their joining as bundles. These two section planes are complementary and are performed if your MRI system does not have a 3D T2 STIR facility, in order to provide high quality, curved, oblique reconstructions [22]. Another benefit of these sequences is that a denervation signal can be seen in muscles. This signal was first described by Polak et al. [23] 15 days after the sciatic nerve had been divided, with an increase in the T1 and T2 relaxation times secondary to increased extracellular water; later on, Hayashi et al. [24] reported a rise in the T2 relaxation time only, 2 weeks after denervation, due to increased blood volume. Other groups have shown an earlier denervation signal at 24 h and 4 days after denervation [25,26]. This signal may last for up to a year after denervation.

3D lava Flex gadolinium coronal sections

The sections are positioned similarly to those in the coronal IDEAL sequence, with a field of vision of 28 cm, thickness of 1.2 mm, slab 60, TR of 7.8, minimum TE and a 288^2 matrix. This sequence allows the three planes of the space to be reconstructed with good spatial imaging, with T1 weighted fat sat gadolinium gradient echo, and also an in phase volume acquisition on post-gadolinium T1 weighted imaging without fat suppression, which also enables multiplanar

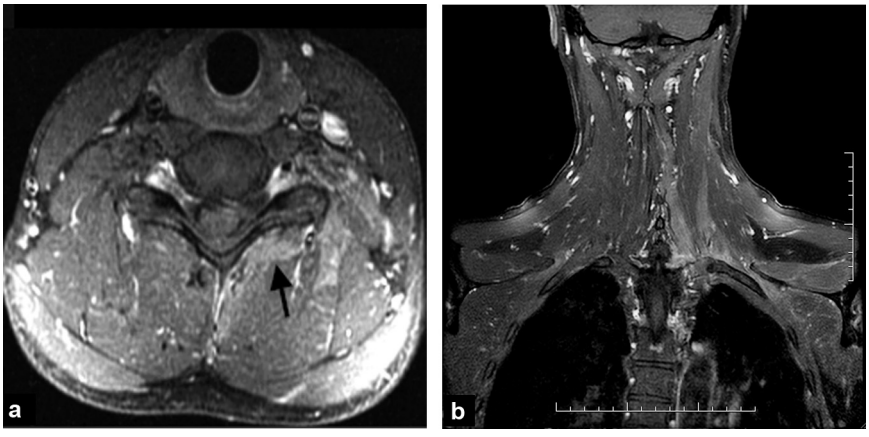

Figure 12. Muscle abnormality, secondary to pre-ganglionic damage: a: the abnormality seen most often is contrast enhancement by the multifidus muscle (black arrow); b: the second abnormality is a T2 weighted hyperintensity. Note the hyperintensity in the left multifidus muscle, located paraspinally and in the more lateral left paravertebral muscle.

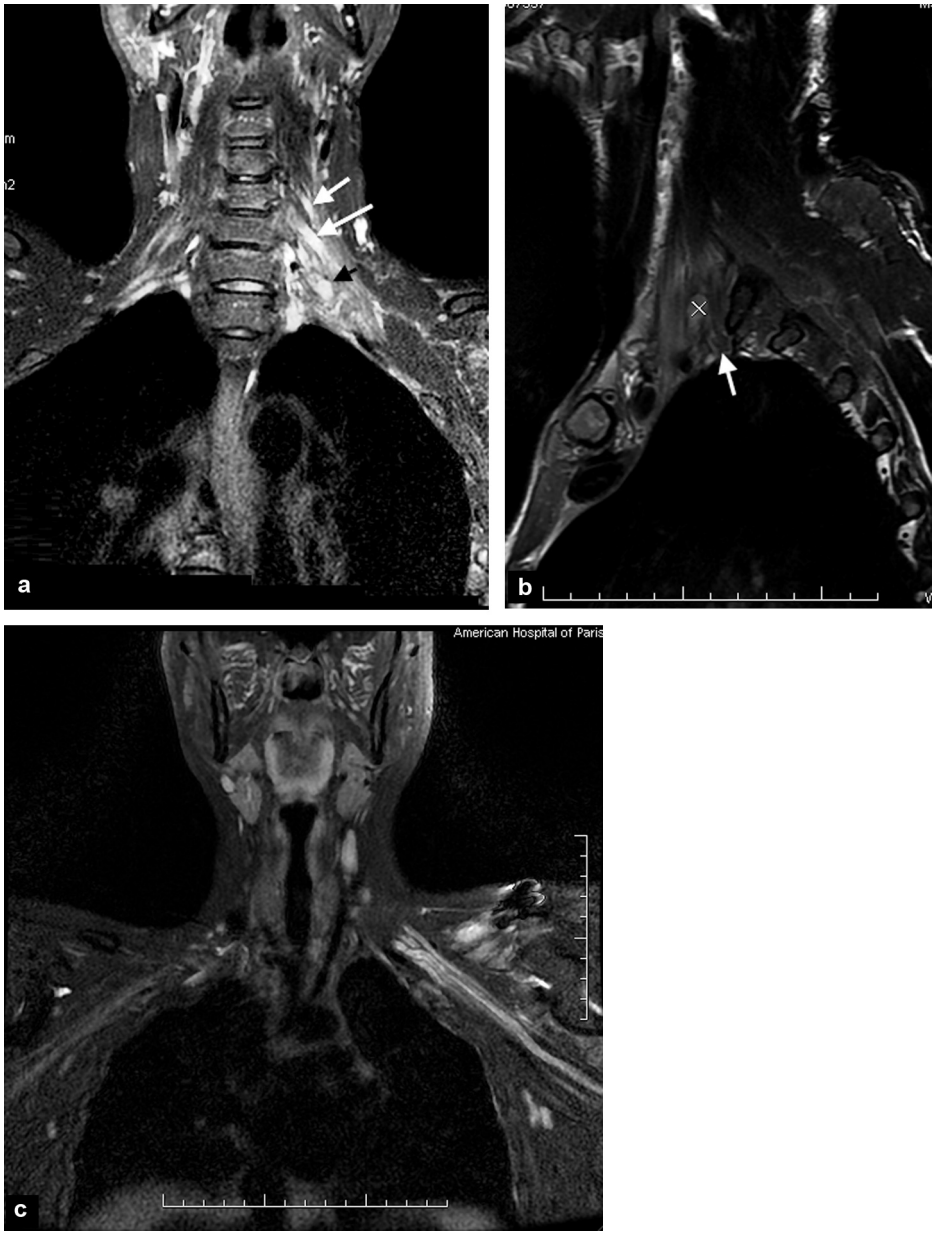

Figure 14. Left brachial plexus damage in the scalene triangle: a: left C5 and C6 root hyperintensity with thickened C6 root (white arrows). Nodular thickening of the C7 root, representing rupture (black arrow); b: nodular thickening of the C7 root (cross) in a T2 weighted sagittal section. Note the normal appearances of the C8 root (white arrow); c: signal abnormality from the left infraclavicular bundles, with no abnormalities in diameter.

reconstruction and good visibility of the various nerve components silhouetted by fat (Fig. 21). Changes in the diameter and signal from the various nerve components compared to the axillary artery can be better identified from these volumes with sections taken in a plane perpendicular to the long axis of the plexus [27]. Nerves can be clearly distinguished from arteries and veins with gadolinium. Curved and oblique reconstructions can also be made, which very clearly individualize the suprascapular nerve (Fig. 22), the region of the trunks with the dorsal scapular artery (Fig. 23), the dividing branches of the trunks and their joining in bundles. Reconstructed axial sections parallel to the middle plane of the discs are used to examine contrast enhancement within the scalene triangle, in the paravertebral muscles and possibly in the spinal canal. Since we have started using this sequence, we no longer carry out an axial T1 weighted fat sat gadolinium sequence along the middle plane of the discs unless significant artefacts are present.

Diffusion weighted MRI

Water diffuses within the nerve fibers anisotropically (one main direction) rather than isotropically (in all directions). This forms the basis of diffusion-weighted imaging (DWI). In diffusion tensor imaging (DTI), the image provides data on the intensity of each voxel and also information in the three

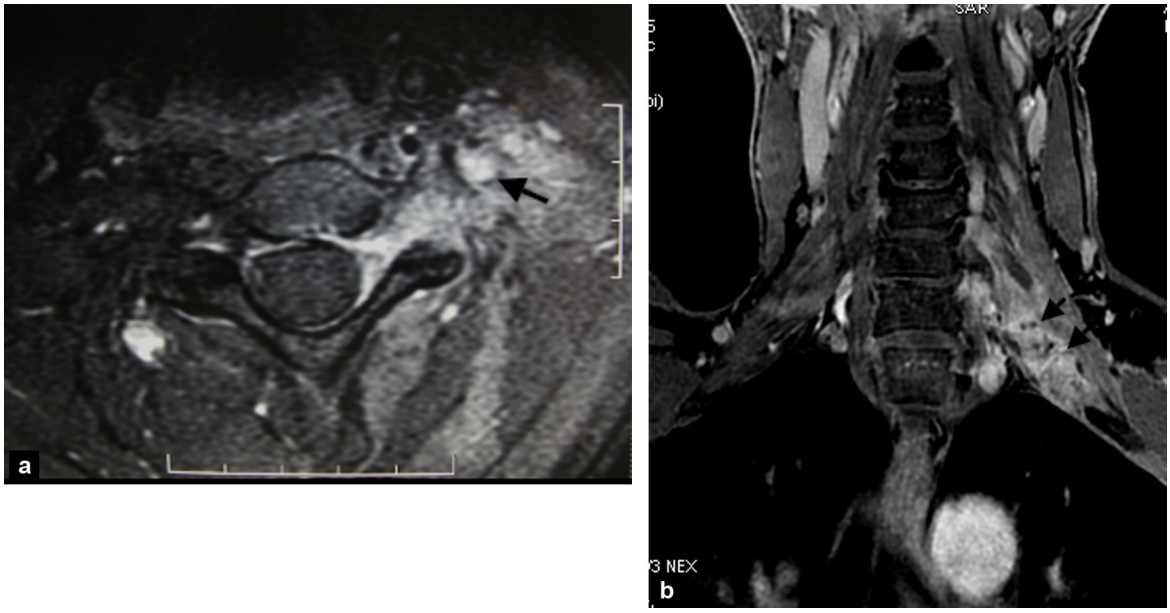

Figure 15. a: contrast enhancement by a retracted spinal ganglion in the scalene triangle (arrow); b: contrast enhancement either side of an intra-scalene C7 rupture. Note the hemosiderin deposits in this gradient echo sequence.

spatial planes of each voxel. Each voxel can be represented by a vector along the main direction of the nerve: the sum of all of these vectors in the volume produces a linear image of the nerve path. Water molecule diffusion is restricted to the axons because of the myelin sheath. Intra-axonal metabolites such as NE (N-Acetyl-Aspartate) and intra-axonal water diffusion is also restricted. Use of a low b factor (< 1000) is more sensitive for the inter-axonal extracellular space [28]. Diffusion weighted imaging visualizes the sensory nerve ganglia, post-ganglionic nerve roots in the scalene triangle, the trunks, and also the lymph nodes. This sequence requires processing with MIP reconstruction in the frontal plane to visualize these neuronal structures and suppress the lymph nodes, which may be superimposed on the neuronal structures as well as possible. This technique does not visualize the nerve roots above C5 or the pre-ganglionic portion of the nerve [15]. The infraclavicular region can be seen in 60% of normal subjects. Reduced signal intensity in traumatic post-ganglionic lesions has been reported [29] and a recent article [17] using diffusion tensor imaging with tractography, reported that intact nerve roots from C5 to T1 were visible on the healthy side in 100% of the patients suffering a plexus injury, with a sensitivity of 88.1% and specificity of 98.8% to diagnose avulsion. The procedure, however, lasts 11 min and 40 s, and cannot therefore be used in everyday practice! A diffusion tensor sequence takes time, both for the acquisition and particularly for processing, thus we do not perform it routinely. The parameters used are a b of 900 and 9 direction gradient or a b of 1000 with 12 direction gradients (some use 30 direction gradients [15]). In practice, we do not find this sequence to be a discriminating one in terms of analysis and we found no signal defect on a post-ganglionic continuity lesion, which produced no response to electrical stimulation preoperatively and therefore reflected intra-fascicular rupture with superficial epineural continuity.

Axillary nerve damage

Review of anatomy and pathology

The sensorimotor axillary nerve is one of the terminal branches of the posterior bundle and runs behind the humeral artery in contact with the anterior region of the subscapularis muscle, before passing from anterior to posterior along an oblique path into the quadrilateral space giving out collaterals to the teres minor, occasionally the subscapularis, the gleno-humeral joint and the sensory branch to the external aspect of the shoulder. It passes around the humerus and then runs along the deep surface of the deltoid muscle, giving out several intramuscular branches, from posterior to anterior. The deltoid is involved in abduction of the arm, antepulsion through its anterior fibers and contributes to extension of the arm via its posterior fibers. The nerve can be damaged in arm traction movements following antero-internal dislocation of the humeral head. One study on 63 patients showed that the damage was due to rupture, usually at the entrance to the quadrilateral space (41/63), where the nerve is fixed inside the space itself (21/63), and a third lesion was identified as a nerve which was continuous but sheathed in the fibrous tissue (14/63) [30]. The axillary nerve is clearly seen on T1 weighted coronal MRI, parallel to the quadrilateral space (QS) (Fig. 24). It appears surrounded by fat, proximal to the space, and in the space itself (Fig. 25). On axial sections it can occasionally be difficult to distinguish it from its accompanying axillary vessels (Fig. 26).

Use of MRI

A prospective study has been carried out on 15 patients with post-traumatic axillary nerve paralysis and found three MRI groups of patients: group 1 had a normal MRI, group

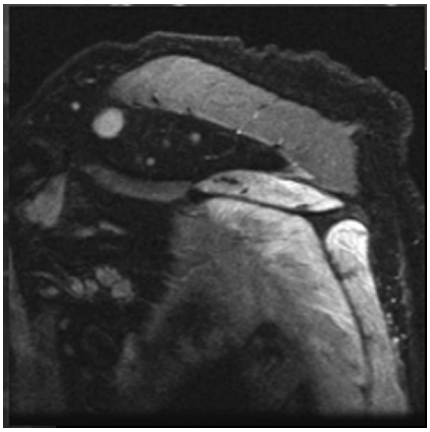

Figure 16. The denervation signal is hyperintense on T2 fat suppression or STIR MRI sequences. Note the supraspinatus, infraspinatus and subscapularis signal abnormalities.

2 had thickening or sheathing of the nerve (fibrosis) at the entrance to, or before the QS (Fig. 27a, b) and in group 3, a neuroma was found on the axillary nerve at the entry to or before the QS. Neuromas are seen as a nodular or oval hyperintense structures on T2 weighted fat sat or STIR MRI, isointense with muscle on T1 weighted MRI, enhancing with gadolinium (Fig. 28a—c). There is a good correlation between radiological, clinical and surgical findings (Table 1). All of the patients with a normal MRI recovered clinically and the neuromas were all confirmed surgically in patients who did not recover clinically. Fibrosis does not predict clinical outcome, as some patients recover functional activity without treatment and others recover functional activity after surgical neurolysis (false negative distal rupture) [31].

The following protocol is used to investigate the axillary nerve:

- axial T1 sections with TR 442 TE 7.5 FOV 28, thickness 4/0, 30 sections;
- axial STIR sections TR 3900 TE 67.6 TI 150 FOV 30, thickness 4/0 30 sections;

Figure 17. Image abnormalities in the left trunks and bundles (black arrow) without abnormal diameters, due to Wallerien degeneration. Note the normal appearance of the right bundles (white arrow).

Figure 18. Left plexus injury. Abnormal signal due to a magic angle of the right brachial plexus roots predominantly in C8 (white arrow).

- quadrilateral space Oblique T1 coronal sections TR 451 TE 7.6 FOV 28, thickness 2/0 12 sections;
- oblique T1 coronal sections after gadolinium injection and axial T1 fat sat sections.

Surgical repair

Nerve surgery

Nerve surgery should ideally be performed within 6 months in order to obtain the best possible results in terms of

Figure 19. Coronal STIR or IDEAL sections in a plane parallel to the long axis of the spine and vertebral bodies covering the spine and vertebrae.

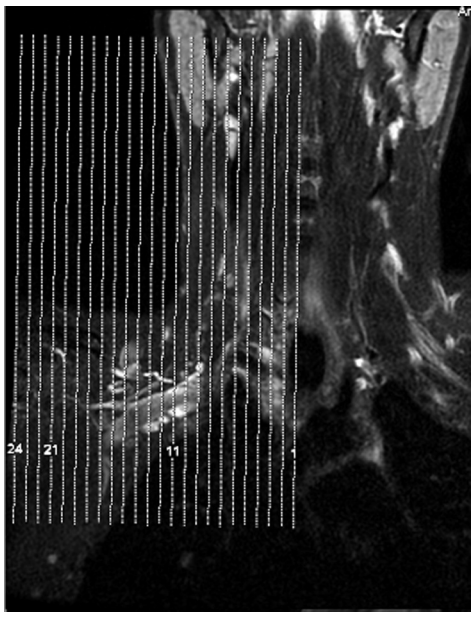

Figure 20. Positioning sagittal T2 weighted fat suppression or IDEAL MRI sections.

recovery. Muscle atrophy, gradual disappearance of the motor end plates and secondary retrograde apoptosis of the dorsal root ganglion neurons [32] make good nerve recovery after 18 months a very poor prospect. There are two approaches, nerve grafts and nerve transfers:

- nerve grafts: these are only possible in ruptures and involve a direct approach to the plexus dividing the nerve root, proximal to the neuroma, until a good microscopic appearance is obtained with the divided root. A donor nerve is then positioned between the root and the nerve or trunk being treated. Mostly, grafting is performed for the most accessible C5 and C6 roots, although the root quality means that the graft is not always reliable. The sural nerve, sensory branch of the radial nerve, cutaneous brachial nerve and vascularized ulnar nerve can be used as grafts. As the ulnar nerve is vascularized, we can harvest it with its superior collateral pedicle and therefore perform

Figure 21. Reconstructions can be made in the different spatial planes from the 3D LAVA sequence which also silhouettes fat which has not been suppressed from the various neuronal components clearly in the in-phase volume.

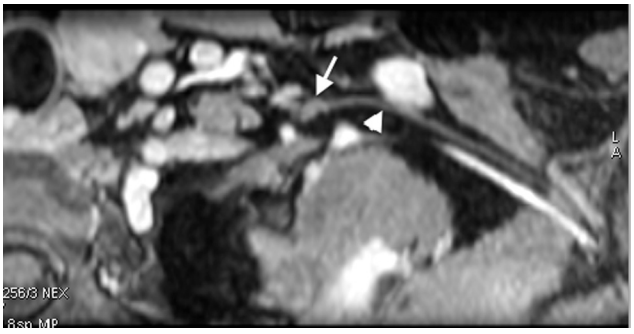

Figure 22. Oblique reconstruction from a 3D lava sequence with fat suppression: the superior trunk is very clearly seen (white arrow) and the suprascapular nerve is seen as far as the supra-coracoid notch (arrow head).

Figure 23. The dorsal scapular artery (white arrow) arises from the subclavian artery (A) and delineates the region of the trunks (black arrow).

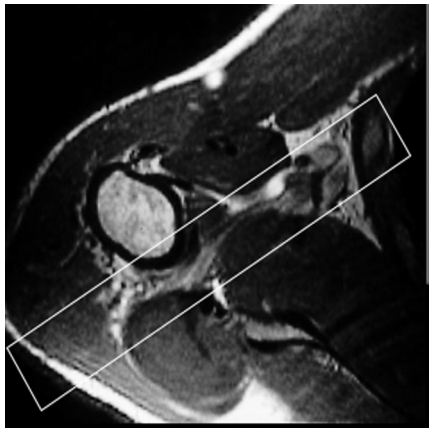

Figure 24. The axis of the axillary nerve is seen on the axial sections, allowing thin sections to be positioned in an oblique coronal plane, which shows the inside of the quadrilateral space.

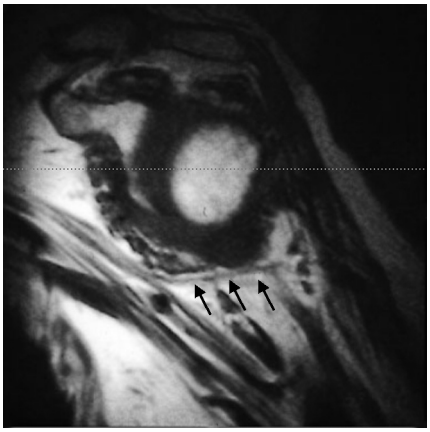

Figure 25. Oblique coronal sections along the axis of the quadrilateral space allow the axillary nerve (black arrows) to be seen clearly, surrounded proximally by fat.

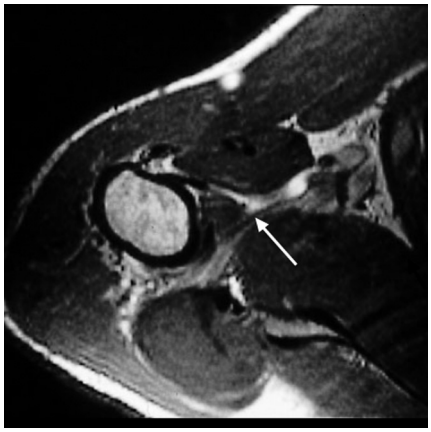

Figure 26. The axillary nerve is seen clearly at the entrance to the quadrilateral space (white arrow) in contact with the subscapularis muscle.

vascularized nerve grafts. This technique is particularly useful in total paralysis and, in some cases, avoids the sural nerves being harvested;

- nerve transfers: this involves connecting a healthy donor nerve (all or part) onto the recipient nerve for targeted restoration of paralyzed functions. There are many possible donor nerves, depending on the function being restored. The transfers which are usually performed are:
  - the external branch of the spinal nerve onto the suprascapular nerve (abduction and rotation of the shoulder),
  - the nerve of the long head of triceps onto the anterior branch of the axillary nerve (abduction and elevation of the shoulder),
  - a bundle of the ulnar nerve onto the bicep nerve (flexion of the elbow),
  - a bundle of the median nerve onto the anterior brachial nerve (flexion of the elbow),
  - three intercostal nerves onto the nerve of the long head of triceps (extension of the elbow),
  - the cutaneous lateral antebrachial nerve onto the dorsal branch of the ulnar nerve (sensation for the ulnar edge of the wrist),
  - one or more bundles of the contralateral C7 nerve root onto the secondary anterolateral trunk or musculocutaneous nerve (elbow flexion) or onto the median nerve (finger flexion).

Another technique involves neurovascularized muscle flaps for elbow flexion and extension.

Palliative surgery

Any surgery other than to the nerve is palliative and includes tendon transfers, arthrodesis and tenodesis.

Palliative surgery is part of a long-term program to improve the functions in a paralyzed limb and can be used to improve the results of direct nerve recovery. Some palliative procedures are simple, although it is difficult to define their indications and each must be considered on an individual case basis. In some situations, humeral derotation osteotomy is preferable to shoulder arthrodesis in almost identical clinical situations.

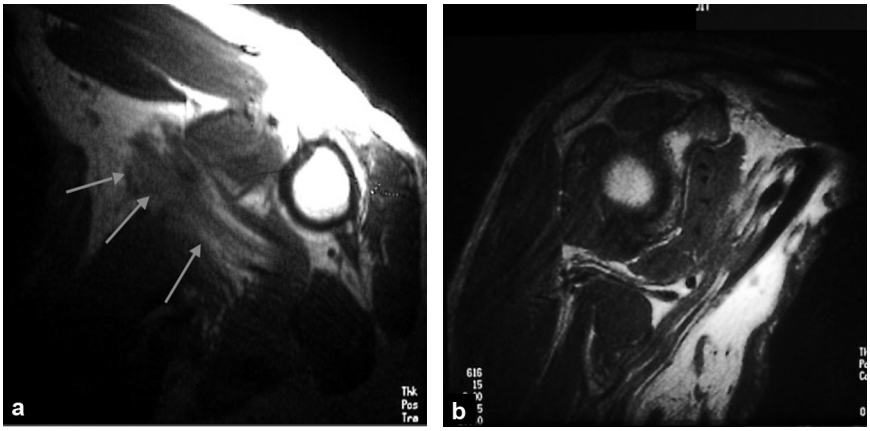

Figure 27. a: T1 weighted hypointense fibrous filling at the entrance to, and in, the quadrilateral space (grey arrows); b: fibrosis is also seen in the oblique coronal plane. Compare with Fig. 25.

Table 1 Correlation between radiological, clinical and surgical findings.

MRI group		Outcome		Operation report	
Group 1	3 cases	Recovered	2	0	
Normal MRI		Lost to follow-up	1	0	
Group 2	8 cases	Recovered	5	0	
Fibrosis		Paralysis	3	Rupture after QS	1
				Neurolysis	2
Group 3	6 cases	Recovered	0		
Neuroma		Paralysis	6	Ruptures before QS with proximal neuroma	6

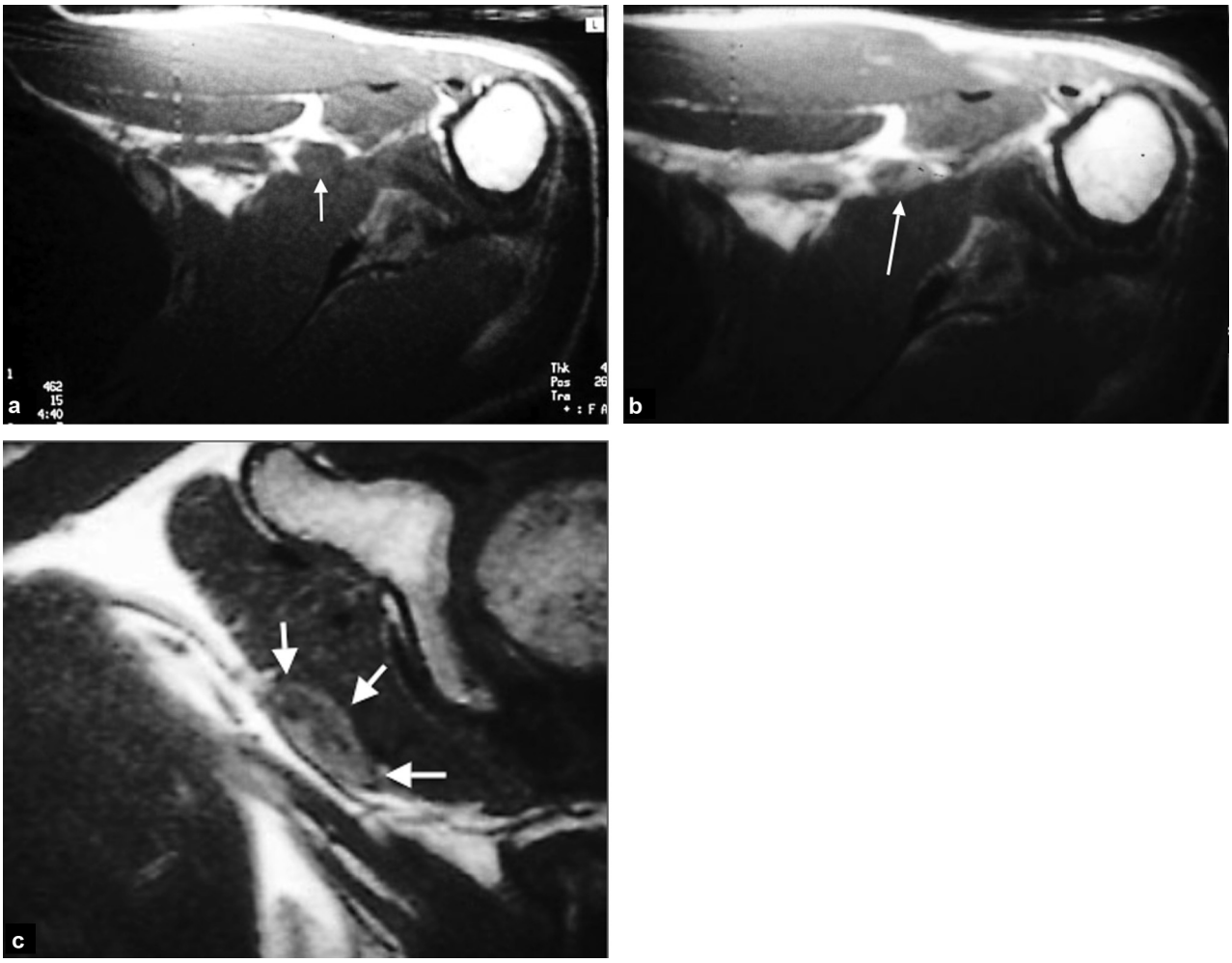

Figure 28. a: neuroma seen as a T1 weighted isointensity in muscle (white arrow) proximal to the quadrilateral space in contact with the subscapularis muscle; b: heterogeneous enhancement of the neuroma on a T1 weighted sequence after injection without fat suppression (white arrow); c: oblong neuroma clearly visible on the oblique coronal section (white arrows).

Treatment strategy

Decisions on treatment should be made according to:
- the type of injury;
- the existence of graftable roots;
- the time since the injury.

Early management is essential, ideally between 1 and 6 months after the initial injury. An abnormal MRI from the first month after the injury can be used to confirm the need for early surgical exploration.

The common belief that pre-ganglionic injuries, which are not accessible for grafting are more serious than post-ganglionic injuries is now believed to be incorrect. Some surgeons carry out targeted transfers from the outset without investigating the nerve roots in the scalene triangle when C5, C6, C7 paralysis is present [33], and others perform both procedures wherever possible [34].

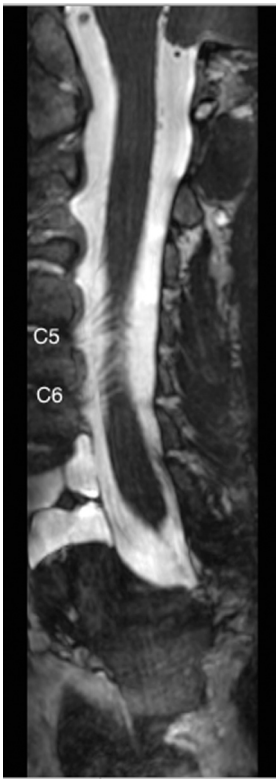

Figure 29. Oblique reconstruction of the posterior rootlets.

Grafts do not produce as good results as targeted nerve transfers, as the donor nerve is also healthy in nerve transfer whereas a graftable root may not be of as good quality. In addition, in nerve transfer the recipient nerve is sutured immediately before its intramuscular branching and therefore no donor nerve fibers are lost in the sensory fibers or those destined for other nerves (no axonal confusion) and only one neuronal suture is performed (unlike a graft, which requires two sutures!).

Preoperative planning may change during the procedure: a root which has not been avulsed may be found to be of very poor quality when it is divided (few or no visible bundles) and a donor nerve for transfer may be damaged in the initial injury (such as the ulnar nerve). Therefore, a change in strategy should always be considered peroperatively, to optimize patient recovery.

In practice, clinical presentations can be divided into partial and total plexus injuries. In partial paralysis (C5/C6/C7), surgeons perform targeted nerve transfers (ulnar biceps, median anterior brachial, triceps axillary nerve, suprascapular spinal, triceps intercostal if damage to C7). In this case, the radiologist should examine the quality of C5 for the possibility of a graft for the shoulder.

In complete plexus paralysis, radiologists should assess the C5 and C6 roots for elbow and hand grafts, in addition to nerve transfers (spinal, intercostal).

Figure 30. IDEAL T2 MRI sequence.

TAKE-HOME MESSAGES

- Pre-ganglionic injuries may be apparent, but it is important to look for minor adverse signs:
  - Total avulsion = avulsion of the anterior and posterior rootlets,
  - Partial avulsion = avulsion of the anterior or posterior rootlets,
  - Pauci-rootlet appearance = the rootlets are visible, but reduced in number compared to the opposite side,
  - Thickened rootlet appearance,
  - Contrast enhancement in the spine or nerve roots.
- Neuronal contrast enhancement in the scalene triangle may be due to:
  - A neuroma in continuity,
  - Rupture,
  - An hematoma around an avulsed root,
  - Contrast enhancement by the retracted ganglion of an avulsed root.
- A brachial plexus T2 weighted hyperintensity may represent reversible endoneurial edema, or reversible or irreversible Wallerien degeneration. The combination of a signal abnormality and increased nerve diameter suggests a poorer prognosis. Functionality cannot be assessed by MRI except when the nerve is divided.
- MRI on its own is of no use except in obvious total avulsion, and needs to be used in tandem with repeated electromyograms to determine the surgical strategy, with or without peroperative stimulation.
- A visible neuroma on the axillary nerve suggests rupture.
- Further surgical correlation information is needed to assess the relevance of contrast enhancement compared to a STIR sequence. Tractography is very useful but needs advances to be made to be less time-consuming.

Clinical case

Total right traumatic paralysis. MRI at 3 months and 1 week. 90° abduction. Fig. 29 shows an oblique reconstruction of

Figure 31. IDEAL T2 MRI sequence.

the posterior rootlets. Figs. 30 and 31 show an IDEAL T2 weighted MRI.

Questions

1. Is it possible to say that the C5 and C6 nerve roots have not been avulsed?
2. Describe the C5 and C6 nerve roots in the scalene triangle.
3. What does the distal fusiform thickening in the C8 pseudomeningocele indicate?

Answers

1. The posterior rootlets are not avulsed, although a full examination is needed on axial reconstructions, looking for partial anterior avulsion, pauci-rootlet appearances or thickened rootlets suggesting pre-ganglionic or ganglion lesion (equivalent of avulsion).
2. The C5 and C6 root signals are abnormal. The C5 root appears to be of normal diameter compared to the C6 root, which is very thickened but does not exhibit nodular thickening. This raises the question of a C6 neuroma in continuity (functional? No signal defect on the diffusion-weighted sequence, contrast enhancement in C6 and slight enhancement of C5 and the superior trunk). No response to peroperative C6 stimulation. The proximal part of C5 is graftable before its attachment to C6. The suprascapular nerve responds to stimulation.
3. The fusiform thickening represents an organized hematoma around the C7 root, which is retracted.

Disclosure of interest

The authors declare that they have no conflicts of interest concerning this article.

References

[1] Rankin JJ. Adult traumatic brachial plexus injury. Clin Radiol 2004;59(9):767—74.
[2] Demondion X, Boutry N, Drizenko A, Paul C, Francke JP, Cotten A. Thoracic outlet anatomic correlation with MRI imaging. AJR Am J Roentgenol 2000;175(2):417—22.
[3] Van Es HW, Bollen TL, van Heesewijk H.P.M. MRI of the brachial plexus: a pictorial review. Eur J Radiol 2010;(74):391—402.
[4] Mizisin AP, Weerasuriya A. Homeostatic regulation of the endoneurial microenvironment during development, aging and in response to trauma, disease and toxic insult. Acta Neuropathol 2011;121:291—312.
[5] Kim DH, Murovic JA, Tiel RL, Kline DG. Infraclavicular brachial plexus stretch injury. Neurosurg Focus 2004;16(5):1—6 [Article 4].
[6] Alnot JY. Traumatic brachial plexus palsy in the adult: retro- and infraclavicular lesions. Clin Orthop 1988;237:9—16.
[7] Seddon HJ. A classification of nerve injuries. Br Med J 1942;29(4260):237—9.
[8] Nagano A, Ochiai N, Sugioka H, Hara T, Tsuyama N. Usefulness of myelography in brachial plexus injuries. J Bone Joint Surg 1989;14:59—64.
[9] Hayashi N, Yamamoto S, Okubo T, Yoshioka N, Shirouzu I, Abe O, et al. Avulsion injury of cervical nerve roots: enhanced intradural nerve roots at MRI imaging. Radiology 1998;206(3):817—22.
[10] Hayashi N, Masumoto T, Abe O, Aoki S, Ohtomo K, Tajiri Y. Accuracy of abnormal paraspinal muscle findings on contrast-enhanced MRI images as indirect signs of unilateral cervical root-avulsion injury. Radiology 2002;223(2):397—402.
[11] Gasparotti R, Ferraresi S, Pinelli L, Crispino M, Pavia M, Bonetti M, et al. Three-dimensional MRI myelography of traumatic injuries of the brachial plexus. AJNR Am J Neuroradiol 1997;18:1733—42.
[12] Doi K, Otsuka K, Okamoto Y, Fujii H, Hattori Y, Baliarsing AS. Cervical nerve root avulsion in brachial plexus injuries: magnetic resonance imaging classification and comparison with myelography and computerized tomography myelography. J Neurosurg 2002;96(3 Suppl.):277—84.
[13] Silbermann-Hoffman O, Goeffroy O, Tubach L, Bensoussan S, Teboul F, Schouman Claeys E. 3D Fiesta-pc MRI myelography of traumatic injuries of the brachial plexus. Scientific poster RSNA; 2003.
[14] Yoshikawa T, Hayashi N, Yamamoto S, Tajiri Y, Yoshioka N, Masumoto T, et al. Brachial plexus injury: clinical manifestations, conventional imaging findings, and the latest imaging techniques. Radiographics 2006;26(1):133—43.
[15] Vargas MI, Viallon M, Nguyen D, Beaulieu JY, Delavelle J, Becker M. New approaches in imaging of the brachial plexus. Eur J Radiol 2010;74(2):403—10.
[16] Tsai PY, Chuang TY, Cheng H, Wu HM, Chang YC, Wang CP. Concordance and discrepancy between electrodiagnosis and magnetic resonance imaging in cervical root avulsion injuries. J Neurotrauma 2006;23(8):1274—81.
[17] Gasparotti R, Lodoli G, Meoded A, Carletti F, Garozzo D, Ferraresi S. Feasibility of diffusion tensor tractography of brachial plexus injuries at 1.5 T. Invest Radiol 2013;48(2):104—12.
[18] Sunderland S. Nerves and nerve injury. Edinburgh: Churchill Livingstone; 1978.
[19] Tagliafico A, Succio G, Serafini G, Martinoli C. Diagnostic accuracy of MRI in adults with suspect brachial plexus lesions: a multicentre retrospective study with surgical findings and clinical follow-up as reference standard. Eur J Radiol 2012;81(10):2666—72.
[20] Chappell KE, Robson MD, Stonebridge-Foster A, Glover A, Allsop JM, Williams AD, et al. Magic angle effects in MRI neurography. AJNR Am J Neuroradiol 2004;25(3):431—40.

[21] Chhabra A, Thawait GK, Soldatos T, Thakkar RS, Grande FD, Chalian M, et al. High-resolution 3T MRI neurography of the brachial plexus and its branches, with emphasis on 3D imaging. AJNR Am J Neuroradiol 2013;34(3):486—97.
[22] Viallon M, Vargas MI, Jlassi H, Lövblad KO, Delavelle J. High-resolution and functional magnetic resonance imaging of the brachial plexus using an isotropic 3D T2 STIR (Short Term Inversion Recovery) SPACE sequence and diffusion tensor imaging. Eur Radiol 2008;18:1018—23.
[23] Polak JF, Jolesz FA, Adams DF. MRI imaging of skeletal muscle: prolongation of T1 and T2 subsequent to denervation. Invest Radiol 1988;23:365—9.
[24] Hayashi Y, Ikata T, Takai H, Takata S, Ishikawa M, Sogabe T, et al. Effect of peripheral nerve injury on nuclear MRI relaxation times of rat skeletal muscle. Invest Radiol 1997;32:135—9.
[25] West GA, Haynor DR, Goodkin, et al. MRI imaging signal intensity changes in denervated muscles after peripheral nerve injury. Neurosurgery 1994;35:1077—86.
[26] Bendszus M, Koltzenburg M, Wessig C, Solymosi L. Sequential MRI imaging of denervated muscle: experimental study. Am J Neuroradiol 2002;23:1427—31.
[27] Sureka J, Cherian RA, Alexander M, Thomas BP. MRI of brachial plexopathies. Clin Radiol 2009;64:208—18.
[28] Le Bihan D, Mangin JF, Poupon C, Clark CA, Pappata S, Molko N, et al. Diffusion tensor imaging: concepts and applications. J Magn Reson Imaging 2001;13(4):534—46.
[29] Takahara T, Hendrikse J, Yamashita T, Mali WP, Kwee TC, Imai Y, et al. Diffusion-weighted MRI neurography of the brachial plexus: feasibility study. Radiology 2008;249(2):653—60.
[30] Lésions du nerf axillaire. Thesis written by Coenes LN 1985 University of Leiden panel chairman Pr Narakas.
[31] Miroux F [Thèse d'exercice de médecine] IRM et pathologie traumatique du nerf axillaire: à propos de 18 observations. Paris: Université Paris-12 Créteil; 1996.
[32] Burnett MG, Zager EL. Pathophysiology of peripheral nerve injury: a brief review. Neurosurg Focus 2004;16(5):1—7 [article 1].
[33] Garg R, Merrell GA, Hillstrom HJ, Wolfe SW. Comparison of nerve transfers and nerve grafting for traumatic upper plexus palsy: a systematic review and analysis. J Bone Joint Surg Am 2011;93(9):819—29.
[34] Sulaiman OA, Kim DD, Burkett C, Kline DG. Nerve transfer surgery for adult brachial plexus injury: a 10-year experience at Louisiana State University. Neurosurgery 2009;65(4 Suppl.):A55—62.